



Investigating a Redox Active Samarium Complex in Catalytic Reactions

Sebastian Kaufmann^[a] and Peter W. Roesky^{*[a]}

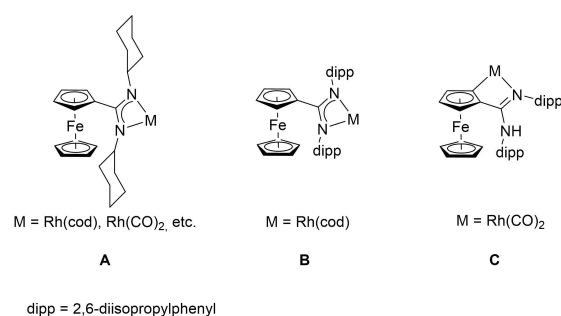
Herein the synthesis of a new ethynyl ferrocenyl amidinate ligand [Fc–C≡C–{C(Ndipp)₂H}] (Fc = ferrocenyl; dipp = diisopropylphenyl) and the subsequent formation of the corresponding samarium amido complex [Sm{Fc–C≡C–{C(Ndipp)₂}₂{N(SiMe₃)₂}] is reported. [Fc–C≡C–{C(Ndipp)₂H}] and [Sm{Fc–C≡C–{C(Ndipp)₂}₂{N(SiMe₃)₂}] were fully characterized including the

study of the complex' redox properties by cyclovoltammetry. Furthermore, we investigated the catalytic properties of the samarium complex in the intramolecular hydroamination reaction and intermolecular dehydrocoupling of pinacol borane with various amines.

1. Introduction

Amidines are very popular ligands because they have the inherent advantage of being easily accessible and show a high flexibility and tunability in terms of their steric demand as well as their electronic properties.^[1–4] These advantages lead to the employment of these ligands for almost any stable metal going from main group^[5–6] over transition metals^[1,7] to f-elements.^[8–12] In lanthanide chemistry, they now compete with the formerly omnipresent cyclopentadienyl ligands in nearly every aspect.^[9,13] Nevertheless, they still have a large potential for further improvements.^[1,5–8,10,14]

Despite the broad scope of substituents, there are only few known examples of amidines functionalized by a ferrocenyl entity in the backbone (Scheme 1, A–C).^[15–18] The corresponding complexes are mainly transitional metal derivatives,^[15–16,19] though there is one report including rare earth elements.^[20] In most of these complexes cyclohexyl substituents are bound to the nitrogen atoms of the amidinate function (Scheme 1, A). Recently, we introduced the more sterically demanding 2,6-diisopropylphenyl (dipp) and mesityl groups as a substituents on the nitrogen atoms.^[18] Owing to the high steric demand, we could alter the coordination mode of the amidinate ligand. Besides the typical k^2N , an *ortho*-metalation of the ferrocene in the backbone was realized by using suitable group 8 metal precursors (Scheme 1, B and C).



Scheme 1. Some examples of known ferrocenyl amidinate complexes and their different binding modes in coordination chemistry.^[16,18]

However, in all these compounds the ferrocenyl substituent is bound directly to the central carbon atom of the amidinate backbone. Herein, we describe the synthesis of a new ethynyl tethered ferrocene dipp amidinate ligand, in which an ethynyl linker is localized between the ferrocene moiety and the dipp amidinate. Due to the remote binding of the ferrocenyl unit there is less steric displacement in the backbone of the ligand, resulting in a release of the steric strain of the ligand. Herein, we showcase the coordination of the new ferrocenyl ethynyl functionalized amidinate ligand to samarium. The resulting complex was subsequently used as a catalyst in intramolecular hydroamination and dehydrocoupling reactions.^[21–27] Furthermore, the redox activity of the ferrocene backbone of the complex was investigated by cyclovoltammetry (CV) as well as in aforementioned catalytic reactions.

2. Results and Discussion

2.1. Synthesis

Since our attempts to coordinate ferrocenyl dipp and mesityl amidines shown in Scheme 1^[18] to the lanthanides failed, we were interested in designing a ligand, which has a lower steric strain upon coordination of the lanthanides. Therefore, we

[a] Dr. S. Kaufmann, Prof. Dr. P. W. Roesky
Institute of Inorganic Chemistry
Karlsruhe Institute of Technology (KIT)
Engesserstrasse 15
76131 Karlsruhe, Germany
E-mail: Roesky@kit.edu
<https://www.aoc.kit.edu/AK> Roesky.php

Supporting information for this article is available on the WWW under <https://doi.org/10.1002/ejic.202100391>

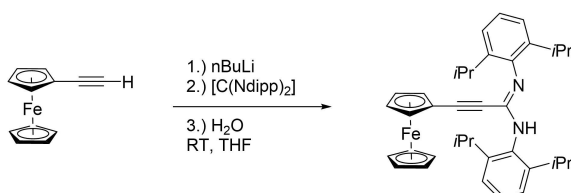
Part of the "Ferrocene Chemistry" Special Collection.

© 2021 The Authors. European Journal of Inorganic Chemistry published by Wiley-VCH GmbH. This is an open access article under the terms of the Creative Commons Attribution Non-Commercial License, which permits use, distribution and reproduction in any medium, provided the original work is properly cited and is not used for commercial purposes.

synthesized a new ethynyl ferrocene amidinate ligand, in which the ferrocene is bridged to the amidinate via an ethynyl function.

The synthesis of this ethynyl ferrocene bis(diisopropylphenyl)amidinate $[Fc-C\equiv C-C(Ndipp)_2H]$ was achieved through an *in situ* lithiation of ethynyl ferrocene,^[28–29] which was followed by subsequent reaction with bis(diisopropylphenyl)carbodiimide (Scheme 2).^[1,15,30] The resulting lithium compound was protonated and recrystallized from hot toluene.

$[Fc-C\equiv C-C(Ndipp)_2H]$ crystallizes in the monomeric space-group *Pn* (Figure 1) with two molecules in the asymmetric unit. The low symmetry of the unit cell is most likely caused by a cocrystallized distorted toluene molecule, which prevents higher symmetry operations. The two molecules form a dimer, which is bridged by hydrogen bonds between the respective imine nitrogen of one amidinate and the amine proton of the other amidinate function. As expected, the amidinate units show a longer bond between the central carbon and the amine (N1-C1 1.338(5) and N1-C1' 1.345(5) Å) and a shorter bond to the imine nitrogen atoms (N2-C1 1.294(5) and N2'-C1' 1.310(4) Å). The dipp-groups are turned towards the ferrocene moiety to avoid a steric clash upon dimerization forming an angle between the amidinate carbon (C1), the amidinate nitrogen and the dipp carbon atom of about 124° at all nitrogen atoms. The ferrocene moieties in the backbone are arranged orthogonally to the amidinate functions.



Scheme 2. Synthesis of $[Fc-C\equiv C-C(Ndipp)_2H]$.

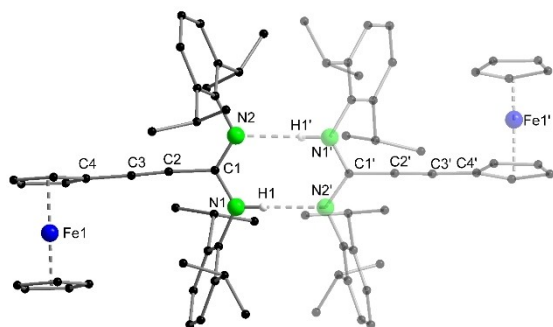


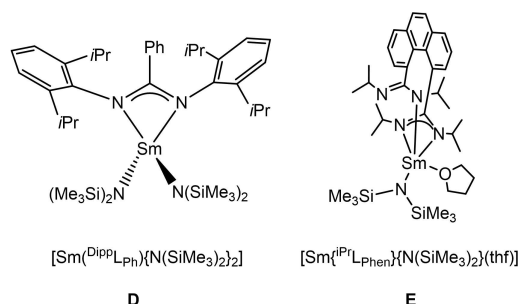
Figure 1. Molecular structure of $[Fc-C\equiv C-C(Ndipp)_2H]$ in solid state. Hydrogen atoms and the second molecule is slightly transparent to show the symmetry. Selected bond lengths [Å] and -angles [°]: N1-C1 1.338(5), N1-C1' 1.345(5), N2-C1 1.294(5), N2'-C1' 1.310(4), C1-C2 1.456(6), C1'-C2' 1.442(5), C2-C3 1.189(5), C2'-C3' 1.198(5), C3-C4 1.442(6), C3'-C4' 1.428(6), N2-C1-N1 119.6(3), N2'-C1'-N1' 118.7(3), C1-N1-C14 126.3(3), C1'-N2'-C14' 121.7(3), C1-N2-C26 122.7(3), C1' N1'-C26'-125.0(3).

The 1H NMR spectrum of $[Fc-C\equiv C-C(Ndipp)_2H]$ exhibits the expected resonances of all functional groups, though DMSO- d_6 is needed as NMR solvent to resolve the signals. Due to the dynamic proton exchange between the nitrogen atoms of the amidine function broad and uninterpretable spectra were obtained in less polar solvents. However, in DMSO- d_6 the resonance of the proton of the amidine function was detected at 8.52 ppm. The $^{13}C\{^1H\}$ NMR spectrum also shows the expected set of signals.

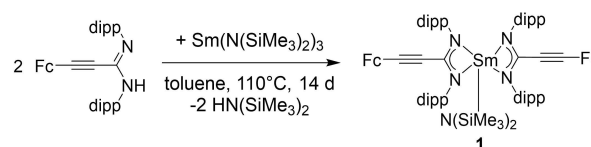
Recently, we reported on samarium amidinate complexes as catalysts for the hydroamination reaction. While the monoamidinate $[Sm^{(Dipp)_{L_{Ph}}}\{N(SiMe_3)_2\}]$ (**D**) was obtained by using the bulky *N,N'*-bis(2,6-diisopropylphenyl)benzamidinate ligand ($^{(Dipp)_{L_{Ph}}}$) (Scheme 3), the bisamidinate samarium compound $[Sm^{(iPr)_{L_{Phen}}}\{N(SiMe_3)_2\}(THF)]$ (**E**) (Scheme 3) was formed by employing the rigid ligand system 4,5-bis(diisopropylamidinate) phenanthrene ($^{(iPr)_{L_{Phen}}}$).^[23–24] Both complexes are functionalized by $N(SiMe_3)_2^-$ groups, which act as leaving groups of the precatalyst in the hydroamination reaction.

For comparison in synthesis and catalysis, we desired to synthesize a related samarium amido complex by using our new ligand $[Fc-C\equiv C-C(Ndipp)_2H]$. Following the synthetic route established for **D** and **E**, we directly reacted two equivalents of the amidine $[Fc-C\equiv C-C(Ndipp)_2H]$ with $[Sm\{N(SiMe_3)_2\}_3]$ to obtain $[Sm\{Fc-C\equiv C-C(Ndipp)_2\}_2\{N(SiMe_3)_2\}]$ (**1**) in 33% yield after recrystallization from hot toluene (Scheme 4). In contrast to **D** a bisamidinate compound is formed. Obviously, the formal substitution of the phenyl group in the amidinate backbone by ethynyl ferrocene reduces the steric bulk of the ligand and thus enables the formation of the bisamidinate samarium complex **1**.

Compound **1** crystallizes in the triclinic space-group $\bar{P}1$ with one molecule in the asymmetric unit (Figure 2). The samarium atom is κ^2N coordinated by two $[Fc-C\equiv C-C(Ndipp)_2]^-$ ligands and one additional $N(SiMe_3)_2^-$, resulting in a distorted square



Scheme 3. The mono and bisamidinate samarium amido complexes $[Sm^{(Dipp)_{L_{Ph}}}\{N(SiMe_3)_2\}_2]$ (**D**) and $[Sm^{(iPr)_{L_{Phen}}}\{N(SiMe_3)_2\}_2(thf)]$ (**E**).^[23–24]



Scheme 4. Synthesis of compound **1**.

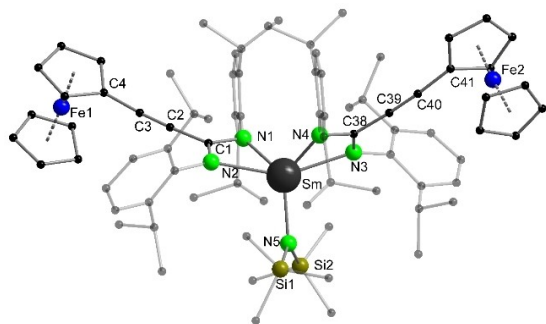


Figure 2. Molecular structure of compound **1** in solid state. Hydrogen atoms are omitted for clarity. Selected bond lengths [Å] and -angles [°]: Sm–N1 2.446(6), Sm–N2 2.459(7), Sm–N3 2.459(6), Sm–N4 2.428(6), Sm–N5 2.245(6), N1–C1 1.326(9), N2–C1 1.344(8), C1–C2 1.450(9), C2–C3 1.188(10), C3–C4 1.418(10), N3–C38 1.329(9), N4–C38 1.343(10), C38–C39 1.441(10), C39–C40 1.190(10), C40–C41 1.437(11), N1–C1–N2 116.9(6), N1–Sm–N2 55.3(2), N2–C1–C2 120.8(7), N1–C1–C2 122.3(6), C1–C2–C3 178.1(9), C2–C3–C4 173.8(10), N3–C38–N4 117.0(7), N4–Sm–N3 55.6(2), N3–C38–C39 122.0(7), N4–C38–C39 121.0(7), C38–C39–C40 176.7(9), C39–C40–C41 176.2(9), N1–Sm–N5 104.7(2), N2–Sm–N5 121.1(2), N3–Sm–N5 121.2(2), N4–Sm–N5 104.2(2), Si1–N5–Si2 124.8(4).

planar pyramid. The bond distances between the samarium atom and the nitrogen atoms of the amidinate units range from 2.428(6) to 2.459(7) Å. Within each amidinate ligand-samarium interaction there is a longer (Sm–N2 2.459(7) Å and Sm–N3 2.459(6) Å) and a shorter bond (Sm–N1 2.446(6) Å and Sm–N4 2.428(6) Å). This bond interactions are in the range of literature known examples (2.28 – 2.52 Å).^[23–24] The samarium nitrogen bond to the N(SiMe₃)₂[–] ligand (Sm–N5 2.249(5) Å) is also in the range of literature known bonds.^[23–24,31–33] Within the amidinate units the delocalisation of charge is confirmed by almost similar bond lengths within the NCN units (N1–C1 1.326(9), N2–C1 1.344(8), N3–C38 1.329(9) and N4–C38 1.343(10) Å). The above mentioned slightly lower steric demand of the ethynyl group in {Fc–C≡C–[C(Ndipp)₂H]} compared to the phenyl group in ^{Dipp}L_{Ph} can be verified by the larger bit angle of {Fc–C≡C–[C(Ndipp)₂H]} (N1–C1–N2 116.9(6) and N3–C38–N4 117.0(7) °) compared to ^{Dipp}L_{Ph} (114.2(4) °).^[24]

On account of the paramagnetic nature of the metal centre, the NMR spectra of compound **1** are quite complex and even in the ¹H, ¹H–COSY and ¹H,¹³C–HMQC NMR spectra not every resonance can be assigned to its corresponding functional group. The resonance of the N(SiMe₃)₂[–] ligand is observed at higher field as expect for a diamagnetic compound (–4.18 ppm). The signals corresponding to the *iso*-propyl groups split and can be seen highfield (–2.51 ppm (4 H)) or downfield shifted (10.32 ppm (2 H) and 12.28 ppm (2 H)), when compared to the precursor (1.27 ppm). In contrast, the signals of the ferrocene unit do not show significant shifts in comparison to [Fc–C≡C–{C(Ndipp)₂H}]. They are detected in the same range as observed in the free ligand (from 4.10 to 4.90 ppm in compound **1**; from 3.93 to 4.27 ppm in [Fc–C≡C–{C(Ndipp)₂H}]). This behavior is a result of the larger distance between the ferrocene units and the paramagnetic center.

The most striking difference in the IR spectra of compounds [Fc–C≡C–{C(Ndipp)₂H}] and **1** is the stretching vibration of the

ethynyl group at 2220 cm^{–1}. While the resonance is broad and split in [Fc–C≡C–{C(Ndipp)₂H}], it is significantly sharper in compound **1**. The measurement of Raman spectra failed as even the lowest laser energy setting melted and destroyed compound **1**.

2.2. Cyclovoltammetry

The electrochemical properties of compound **1** were investigated by cyclovoltammetric measurements. The cyclovoltammogram in Figure 3 shows a quasireversible redox wave at E⁰_{1/2} = 119 mV (ΔE = 83 mV, i_{pc}/i_{pa} = 0.87). Despite two ferrocenyl moieties present in compound **1** only one redox event can be observed in the cyclovoltammogram. This indicates a chemical independency of each ferrocene group. In comparison to our previously published ferrocenyl amidinate complexes, e.g., **B** (Figure 1), we see a comparable anodically shifted potential (**1**: 119 mV vs. [Fc{C(Ndipp)₂Rh(CO)₂}: 223 mV or [Fc{C(Ndipp)₂Rh(cod)}]: 138 mV).^[18]

Next, we tried to replicate these electrochemical observations chemically by employing different oxidizing agents. In almost all cases this led to an insoluble powder, which could not be further characterized. Only the usage of [Ag(OC(CF₃)₃)₄] yielded a soluble species, which could not be recrystallized or further analysed and decomposed upon reduction with different reducing agents.

2.3. Catalysis

To study the newly designed ferrocene functionalized amidinate in hydroamination catalysis we compared compound **1** with the established mono- and bisamidinate samarium complexes **D** and **E** (Scheme 3). Although these systems are different either in terms of the number of ligands or the

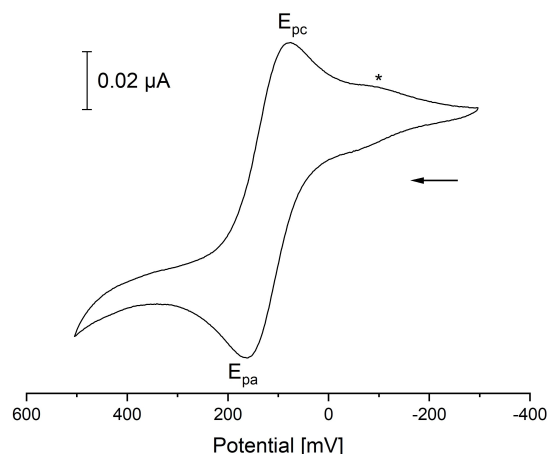


Figure 3. Excerpt from the cyclovoltammogram of compound **1** at room temperature in CH₂Cl₂ (vs. Fc/Fc⁺; v = 10 mV s^{–1}, Pt/[Bu₄N][PF₆]/Ag). The asterisk wave is an artefact of the solvent. At currents greater 600 mV the decomposition of the solvent was observed.

substituents attached to the nitrogen atom, we intended to see some general trends. Table 1 shows the results of the cyclisation of several aminoalkanes and an amino alkyne by using **1** as catalyst. The catalyst was active in all reactions, the products were formed under relatively mild conditions and the reactions yielded very good to quantitative yields. The experiments were carried out under rigorously anaerobic reaction conditions in C_6D_6 at 25 °C or 60 °C, respectively, with a catalyst loading of 5 mol%.

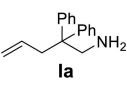
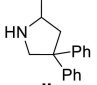
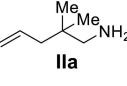
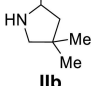
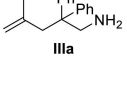
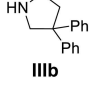
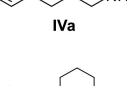
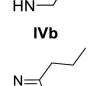
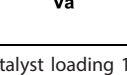
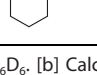
As expected, the cyclisation of the amino substrates is substrate depended. As a general observation one can summarize that the intramolecular hydroamination with compound **1** as catalyst is faster for the formation of smaller rings. The rate increase by having bulky substituents in β -carbon position (Thorpe-Ingold effect)^[34] and smaller substituents bound to the double bond. This leads to the following trend within our reaction series: **Ia** = **Va** > **Ila** > **Iva** > **IIla**. The reaction of **Ia** and **Va** to the respective products occurs at room temperature and the 1H NMR shows full conversion after a few minutes. The other substrates needed higher reaction temperature to boost the cyclisation process. Due to the still slower reaction times, kinetic studies of the occurring reactions could be performed by using continuous measurement of 1H NMR spectra. These kinetic measurements were applied for the reactions of **Ila**, **IIla** and **Iva**. By plotting the relative substrate concentration of **II** and **III** against the time, a linear dependency was seen, which indicates a zero-order kinetics with respect to the substrate concentration within the range of 85–10% relative substrate concentration (see SI Figure S9 and Figure S10). In contrast for **Iva**, the formation of six membered ring, the analysis of the graph leads to a first order kinetic with respect to the substrate concentration (see SI Figure S11).

If we compare the reaction times with those of our previously reported samarium catalysts **D** and **E**,^[23–24] we can see a different behavior for each reaction. Comparing reaction **II** to our previous results shows that **1** is slower than the monoamidante system **D** but faster than the bisamidante **E**. Additionally, we reported kinetics for this reaction before and observe a reaction of first order in respect to the substrate concentration. This contrasts with the observations with **1**, where we observed zero-order kinetics. On the other hand, compound **1** is slower than **D** and **E** in the cyclization reaction of **III** and **IV**. Also, a difference in the kinetics is observed for the reactions of **Iva**. By using **D** and **E** as catalysts, we observed zero order kinetics, while first order kinetics with respect to the substrate are observed by using **1**. While **1** is rather sluggish for the transformation of **IIla** and **Iva** the complete opposite is observed in the reaction of **Va**. Here, compound **1** outperforms catalysts **D** and **E**.^[23–24] In summary, we see a strong substrate dependency in terms of speed and kinetics. Although **1**, **D** and **E** are all samarium amidinate complexes, the slight differences in the ligand appear to have a greater impact on catalytic performance than expected.

Besides the well-known intramolecular hydroamination reaction, we also investigated compound **1** as catalyst in the intermolecular dehydrocoupling (Table 2).^[26–27,35–37] All reactions display a fast and clean conversion independent of the amine substrate used. If we compare our results to previously reported catalysts used in this reaction, we see that our rather bulky heterobimetallic amidinate compound achieves the same reaction times as alkaline metal and earth alkaline metal complexes reported with a β -diketiminato ligand.^[26–27,38–39]

Finally, we investigated an *in-situ* oxidation of the ferrocene moiety of compound **1** to study the influence of the oxidized

Table 1. Hydroamination of amino alkenes and an amino alkyne with compound **1** as a catalyst.^[a]

Nr.	Substrate	Product	T [°C]	T [min]	Conversion[b] [%]
1			25	< 5	> 97
2			60	80	> 88
3			60	200	> 98
4			60	120	> 98
5			25	< 5	> 98

[a] Reaction conditions: catalyst loading 10–15 mg (5 mol%), C_6D_6 . [b] Calculated with ferrocene as an internal standard.

Table 2. Dehydrocoupling of different amines with pinacol borane in the presence of compound **1** as a catalyst.^[a]

Nr	Substrate	Product	T [°C]	t [min]	Conversion ^[b] [%]
1			25	< 5	> 99
2			25	< 5	> 99
3			25	< 5	> 99
4			25	< 5	> 99

[a] Reaction conditions: catalyst loading 10–15 mg (5 mol%), C₆D₆. [b] Calculated using the ¹¹B NMR spectrum (no visible substrate).

species onto the catalytic properties. Upon oxidation of the catalyst a complete deactivation of its catalytic abilities was seen, even after prolonged heating of the reaction mixture (switching-off). However, a reactivation (switching-on) with various reducing agents was not possible.

3. Summary

In summary, we presented a new ethynyl ferrocenyl amidine and its corresponding samarium amido complex **1**. Compound **1** was investigated in terms of its catalytic properties in intramolecular hydroamination and intermolecular dehydrocoupling. By comparing **1** with the related samarium catalysts **D** and **E** the slight differences in the ligands appear to have a great impact on catalytic performance and kinetics in hydroamination catalysis. The activity of **1** is in the range of literature known examples. For the intermolecular dehydrocoupling of different amines with pinacol borane **1** shows a very high activity, which is in the range of the most active systems reported so far. *In situ* oxidation of the **1** terminates its activity in both catalytic conversions. Attempts to reduce this inactive species back to the catalytic active form of **1** failed.

Experimental section

General Procedures

All manipulations were performed under exclusion of moisture and oxygen in flame-dried Schlenk-type glassware or in an argon-filled MBraun glovebox. Toluene was dried using a MBraun solvent purification system (SPS-800). THF was distilled under nitrogen from potassium/benzophenone prior to use. C₆D₆ was vacuum transferred from sodium/potassium alloy into thoroughly dried glassware with the probe substance and flame sealed afterwards. Solution NMR spectra were recorded with NMR instruments operating at ¹H Larmor frequencies of 300 and 400 MHz. ¹H and ¹³C {¹H} chemical shifts were referenced to the residual ¹H and ¹³C resonances of the deuterated solvents and are reported relative to tetramethyl silane (TMS). Coupling constants J are given in Hertz as

positive values, regardless of their actual individual signs. The multiplicity of the signals is indicated as s, d, q, or m for singlets, doublets, quartets, or multiplets, respectively. The abbreviation bs is given for broadened signals. IR spectra were obtained on a Bruker Tensor 37 FTIR spectrometer equipped with a room temperature DLATGS detector and a diamond ATR (attenuated total reflection) unit. IR spectra were recorded using the IR spectrometer in the range from 4000 to 400 cm⁻¹ using a KBr beam splitter. Samples were measured by using the attenuated total reflection (ATR) technique on bulk material. Cyclic voltammetry measurements were performed with a suitable potentiostat and electrochemical cell within a glovebox. We used a freshly polished Pt disk working electrode, a Pt wire as counter electrode, and an Ag wire as (pseudo) reference electrode [[nBu₄N][PF₆] (0.1 M) as electrolyte]. Potentials were calibrated against the Fc/Fc⁺ couple (internal standard). Elemental analyses were carried out with a Micro Cube from Elementar Analysensysteme GmbH. Because of the air-sensitive nature of some reported complexes, only slightly deviating elemental analyses could be obtained. Experimental procedure for X-ray analysis is given in the Supporting Information. For information on the catalysis and the kinetic measurements consult the Supporting Information.

Ethynyl ferrocene^[40] and [Sm{N(SiMe₃)₂}₃]^[41] were synthesized according to literature known methods. All other reagents were used as received without further purification.

Synthesis of [Fc-C≡C-{C(Ndip)₂H}]

1.00 g Ethynylferrocene (4.76 mmol, 1.00 eq.) was dissolved in 25 mL of thf and 1.90 mL of n-butyllithium (4.76 mmol, 1.00 eq.) were added via syringe at -88 °C.^[30] After stirring the reaction mixture for one hour at room temperature, the mixture was cooled again to -88 °C and 1.73 g 2,6-diisopropylphenylcarbodiimid (4.76 mmol, 1.00 eq.) were added. After stirring the mixture for twelve hours at room temperature, 20 mL of water were added to protonate the ligand. The organic phase was separated, washed with brine and dried over sodium sulphate. The solvent was then removed *in vacuo* and the product was obtained as an orange solid. Yield: 90% (2.45 g, 4.28 mmol).

¹H NMR (DMSO-d₆, 300 MHz, 25 °C): δ [ppm] = 1.19–1.27 (m, 24 H, *i*Pr-CH₃), 3.01 (bs, 2 H, *i*Pr-CH), 3.77 (bs, 2 H, *i*Pr-CH), 3.93 (s, 5 H, Cp), 4.22 (s, 2 H, Cp_{sub}), 4.27 (s, 2 H, Cp_{sub}), 6.92–7.12 (m, 6 H, Ph), 8.52 (s, 1 H, NH). ¹³C {¹H} NMR (DMSO-d₆, 75 MHz, 25 °C): δ [ppm] = 22.3 (*i*Pr-CH), 23.4 (*i*Pr-CH₃), 24.4 (*i*Pr-CH₃), 25.3 (*i*Pr-CH), 27.2 (*i*Pr-CH₃), 28.1

(*iPr*-CH₃) 61.6 (C_p_{sub}), 69.2 (C_p_{sub}), 69.4 (C≡C), 69.7 (Cp), 71.1 (C≡C), 90.7 (q-Cp), 122.3 (dipp), 122.7 (dipp), 127.4 (dipp), 129.4 (dipp), 133.5 (dipp), 138.9 (dipp) 146.8z (NCN). IR (ATR, ν, cm⁻¹): 1320 (w, ν_{C-H}), 1360 (w, ν_{C-H}), 1380 (w, ν_{C-H}), 1439 (w, ν_{C-H}), 1462 (m, ν_{C-H}), 1584 (m, ν_{C-Car}), 1611 (s, ν_{C-Car}), 2163 (w, ν_{C≡C}), 2205 (w, ν_{C≡C}), 2866 (m, ν_{C-H}), 2960 (s, ν_{C-H}). Elemental analysis (calcd for C₃₇H₄₄FeN₂) [%]: C 77.23 (77.61), H 7.56 (7.75), N 4.51 (4.53).

Synthesis of [Sm{Fc-C≡C-C(Ndipp)}₂{N(SiMe₃)₂}]

200 mg [Fc-C≡C-C(NHdipp)(Ndipp)] (0.349 mmol, 2.00 eq.) and 119 mg [Sm{N(SiMe₃)₂}₃] (0.175 mmol, 1.00 eq.) were combined in a Schlenk flask and dissolved in 15 mL of toluene.^[30] The reaction mixture was heated to 110 °C and stirred for ten days. Afterwards, the solvent was removed *in vacuo* and the residue was washed several times with *n*-pentane. The residue could be recrystallized from hot toluene to yield X-ray suitable crystals. Single crystalline yield: 33% (84 mg, 0.0581 mmol).

¹H NMR (300 MHz, C₆D₆, 25 °C): δ [ppm] = -4.85 (bs, 6 H, *iPr*-CH₃), -4.18 (bs, 18 z H, SiMe₃), -2.51 (s, 4 H, *iPr*-CH), -2.34 (bs, 3 H, *iPr*-CH₃), 1.47 (m, 12 H, *iPr*-CH₃), 2.00 (s, 6 H, *iPr*-CH₃), 2.91 (s, 6 H, *iPr*-CH₃), 3.61 (m, 12 H, *iPr*-CH₃), 3.76 (s, 4 H, C_p_{sub}), 4.13 (s, 3 H, *iPr*-CH₃), 4.17 (s, 6 H, *iPr*-CH₃), 4.34 (s, 10 H, Cp), 4.73 (s, 2 H, C_p_{sub}), 4.85 (s, 2 H, C_p_{sub}), 5.52 (bs, 4 H, dipp), 6.58 (bs, 2 H, dipp), 6.91 (bs, 2 H, dipp), 7.03 (bs, 2 H, dipp), 7.96 (bs, 2 H, dipp), 10.32 (s, 2 H, *iPr*-CH), 12.27 (s, 2 H, *iPr*-CH). ¹³C{¹H} NMR (75 MHz, C₆D₆, 25 °C): δ [ppm] = 2.7 (SiMe₃), 21.4 (*iPr*-CH₃), 24.4 (*iPr*-CH₃), 24.4 (*iPr*-CH₃), 26.2 (*iPr*-CH), 26.5 (*iPr*-CH₃), 27.3 (*iPr*-CH₃), 28.6 (*iPr*-CH₃), 30.2 (*iPr*-CH₃), 32.6 (*iPr*-CH), 33.3 (*iPr*-CH), 64.3 (q-C), 70.3 (C_p_{sub}), 70.6 (Cp), 72.4 (C_p_{sub}), 72.8 (C_p_{sub}), 87.4 (q-C), 104.2 (q-C), 122.7 (dipp), 123.4 (dipp), 125.5 (dipp). The resonances of the quaternary carbon atoms could not be assigned to their respective functional groups due to paramagnetic shifting. ¹H,¹H-COSY and ¹H,¹³C-HMQC experiment were used to assign the functional groups to the respective signals (see SI for more information). IR (ATR, ν, cm⁻¹): 1360 (w, ν_{C-H}), 1382 (w, ν_{C-H}), 1462 (m, ν_{C-H}), 1585 (s, ν_{C-Car}), 1615 (w, ν_{C-N}), 2216 (s, ν_{C≡C}), 2866 (w, ν_{C-H}), 2927 (m, ν_{C-H}), 2958 (m, ν_{C-H}). Elemental analysis (calcd for C₈₀H₁₀₄Fe₂N₅Si₂Sm) [%]: C 65.56 (66.09), H 6.59 (7.21), N 4.58 (4.82); elemental analysis gave reproducibly low carbon and proton values. High-res mass was not possible due to the heavy molar weight of the compound.

Supporting Information

(see footnote on the first page of this article) NMR and IR spectra, kinetic measurements, XRD data and ORTEP plots.

Deposition Numbers 2082238 (for [Fc-C≡C-C(Ndipp)₂H]), and 2082239 (for 1) contain the supplementary crystallographic data for this paper. These data are provided free of charge by the joint Cambridge Crystallographic Data Centre and Fachinformationszentrum Karlsruhe Access Structures service www.ccdc.cam.ac.uk/structures.

Acknowledgements

The financial support by the DFG funded Collaborative Research Centre CRC/Transregio 88, "Cooperative effects in homo- and heterometallic complexes (3MET)" project B3 is gratefully acknowledged. Dr. T. Brunner and L. Hartenstein are acknowledged for their support in synthesizing the substrates for catalysis and T.

Schon is acknowledged for his support during catalytic measurements. We thank Dr. M. T. Gamer for his help with the crystal structure refinement. We thank Prof. Dr. F. Breher for the possibility to measure the cyclovoltammographic measurements at his device. Additionally, we thank Dr. M. Radius for the introduction into the apparatus. Open access funding enabled and organized by Projekt DEAL.

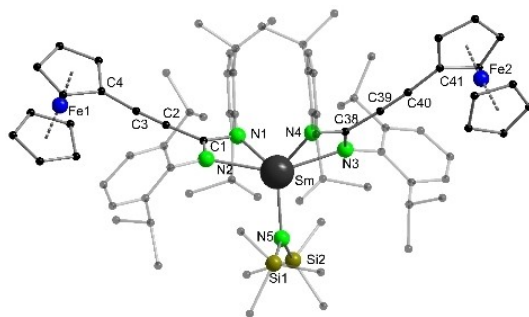
Conflict of Interest

There are no conflicts to declare.

Keywords: Lanthanides · Homogeneous catalysis · N ligands · Ligand design · Cyclic voltammetry

- [1] F. T. Edelmann, in *Adv. Organomet. Chem.*, Vol. 57 (Eds.: A. F. Hill, M. J. Fink), Academic Press, 2008, pp. 183.
- [2] S.-i. Ogata, A. Mochizuki, M.-a. Kakimoto, Y. Imai, *Bull. Chem. Soc. Jpn.* 1986, 59, 2171.
- [3] M. P. Coles, *Dalton Trans.* 2006, 985.
- [4] S. Bamber, M. W. Bouwkamp, A. Meetsma, B. Hessen, *J. Am. Chem. Soc.* 2004, 126, 9182.
- [5] M. Asay, C. Jones, M. Driess, *Chem. Rev.* 2011, 111, 354.
- [6] S. Khoo, H. X. Yeong, Y. Li, R. Ganguly, C. W. So, *Inorg. Chem.* 2015, 54, 9968.
- [7] P. C. Junk, M. L. Cole, *Chem. Commun.* 2007, 1579.
- [8] F. T. Edelmann, *Chem. Soc. Rev.* 2012, 41, 7657.
- [9] F. T. Edelmann, *Coord. Chem. Rev.* 2018, 370, 129.
- [10] F. T. Edelmann, *Coord. Chem. Rev.* 1994, 137, 403.
- [11] F. T. Edelmann, D. M. M. Freckmann, H. Schumann, *Chem. Rev.* 2002, 102, 1851.
- [12] F. T. Edelmann, *Chem. Soc. Rev.* 2009, 38, 2253.
- [13] F. T. Edelmann, *Angew. Chem.* 1995, 34, 2466.
- [14] A. A. Trifonov, *Coord. Chem. Rev.* 2010, 254, 1327.
- [15] J. R. Hagadorn, J. Arnold, *Inorg. Chem.* 1997, 36, 132.
- [16] J. R. Hagadorn, J. Arnold, *J. Organomet. Chem.* 2001, 637, 521.
- [17] N. Dastagiri Reddy, P. E. Fanwick, R. A. Walton, *Inorg. Chim. Acta* 2001, 319, 224.
- [18] S. Kaufmann, M. Radius, E. Moos, F. Breher, P. W. Roesky, *Organometallics* 2019, 38, 1721.
- [19] K. Multani, L. J. E. Stanlake, D. W. Stephan, *Dalton Trans.* 2010, 39, 8957.
- [20] Y. Luo, Z. Gao, J. Chen, *J. Organomet. Chem.* 2017, 846, 18.
- [21] P. Benndorf, J. Jenter, L. Zielke, P. W. Roesky, *Chem. Commun.* 2011, 47, 2574.
- [22] P. Benndorf, J. Kratsch, L. Hartenstein, C. M. Preuss, P. W. Roesky, *Chem. Eur. J.* 2012, 18, 14454.
- [23] N. Kazeminejad, D. Munzel, M. T. Gamer, P. W. Roesky, *Chem. Commun.* 2017, 53, 1060.
- [24] N. Kazeminejad, L. Münzfeld, M. T. Gamer, P. W. Roesky, *Dalton Trans.* 2019, 48, 8153.
- [25] J. Jenter, R. Köppe, P. W. Roesky, *Organometallics* 2011, 30, 1404.
- [26] A. Harinath, S. Anga, T. K. Panda, *RSC Adv.* 2016, 6, 35648.
- [27] A. Harinath, J. Bhattacharjee, H. P. Nayek, T. K. Panda, *Dalton Trans.* 2018, 47, 12613.
- [28] T. Baumgartner, M. Fiege, F. Pontzen, R. Arteaga-Müller, *Organometallics* 2006, 25, 5657.
- [29] T. P. Seifert, J. Klein, M. T. Gamer, N. D. Knöfel, T. J. Feuerstein, B. Sarkar, P. W. Roesky, *Inorg. Chem.* 2019, 58, 2997.
- [30] S. Kaufmann, Dissertation thesis, Karlsruher Institut für Technologie (KIT) (Göttingen), 2020.
- [31] C. Cui, A. Shafir, J. A. R. Schmidt, A. G. Oliver, J. Arnold, *Dalton Trans.* 2005, 1387.
- [32] G. B. Deacon, C. M. Forsyth, P. C. Junk, J. Wang, *Inorg. Chem.* 2007, 46, 10022.
- [33] P. Liu, Y. Zhang, Y. Yao, Q. Shen, *Organometallics* 2012, 31, 1017.
- [34] R. M. Beesley, C. K. Ingold, J. F. Thorpe, *J. Chem. Soc. Trans.* 1915, 107, 1080.

- [35] S. Hong, T. J. Marks, *Acc. Chem. Res.* **2004**, *37*, 673.
[36] M. R. Gagne, L. Brard, V. P. Conticello, M. A. Giardello, C. L. Stern, T. J. Marks, *Organometallics* **1992**, *11*, 2003.
[37] M. R. Gagne, C. L. Stern, T. J. Marks, *J. Am. Chem. Soc.* **1992**, *114*, 275.
[38] D. F. Schreiber, C. O'Connor, C. Grave, Y. Ortin, H. Müller-Bunz, A. D. Phillips, *ACS Catal.* **2012**, *2*, 2505.
[39] D. J. Liptrot, M. S. Hill, M. F. Mahon, A. S. S. Wilson, *Angew. Chem. Int. Ed.* **2015**, *54*, 13362.
[40] J. Polin, H. Schottenberger, *Org. Synth.* **1996**, *73*, 262.
- [41] D. C. Bradley, J. S. Ghotra, F. A. Hart, *J. Chem. Soc. Chem. Commun.* **1972**, 349.
-
- Manuscript received: May 7, 2021
Revised manuscript received: May 28, 2021
Accepted manuscript online: June 1, 2021
-



*Dr. S. Kaufmann, Prof. Dr. P. W. Roesky**

1 – 8

**Investigating a Redox Active
Samarium Complex in Catalytic
Reactions**



We present the synthesis of a new ethynyl ferrocene amidinate and its samarium complex. Additionally, we studied the redox properties of the

samarium complex and investigated its catalytic properties in hydroamination and dehydrocoupling catalysis.
